Specific cardiolipin–SecY interactions are required for proton-motive force stimulation of protein secretion

Robin A. Corey[a,1], Euan Pyle[b,c,2], William J. Allen[a,2], Daniel W. Watkins[a], Marina Casiraghi[d], Bruno Miroux[d], Ignacio Arechaga[e,f], Argyris Politis[b], and Ian Collinson[a,3]

[a]School of Biochemistry, University of Bristol, Bristol BS8 1TD, United Kingdom; [b]Department of Chemistry, King's College London, London SE1 1DB, United Kingdom; [c]Department of Chemistry, Imperial College London, SW7 2AZ London, United Kingdom; [d]Laboratoire de Biologie Physico-Chimique des Protéines Membranaires, Institut de Biologie Physico-Chimique, CNRS, Université Paris Diderot, Sorbonne Paris Cité University, PSL Research University, 75005 Paris, France; [e]Departamento de Biología Molecular, Universidad de Cantabria–Consejo Superior de Investigaciones Científicas (CSIC)-Sociedad para el Desarrollo Regional de Cantabria (SODDERCAN), 39011 Santander, Spain; and [f]Instituto de Biomedicina y Biotecnología de Cantabria, Universidad de Cantabria–CSIC-SODERCAN, 39011 Santander, Spain

Edited by William T. Wickner, Geisel School of Medicine at Dartmouth College, Hanover, NH, and approved June 22, 2018 (received for review December 12, 2017)

The transport of proteins across or into membranes is a vital biological process, achieved in every cell by the conserved Sec machinery. In bacteria, SecYEG combines with the SecA motor protein for secretion of preproteins across the plasma membrane, powered by ATP hydrolysis and the transmembrane proton-motive force (PMF). The activities of SecYEG and SecA are modulated by membrane lipids, particularly cardiolipin (CL), a specialized phospholipid known to associate with a range of energy-transducing machines. Here, we identify two specific CL binding sites on the *Thermotoga maritima* SecA–SecYEG complex, through application of coarse-grained molecular dynamics simulations. We validate the computational data and demonstrate the conserved nature of the binding sites using in vitro mutagenesis, native mass spectrometry, biochemical analysis, and fluorescence spectroscopy of *Escherichia coli* SecYEG. The results show that the two sites account for the preponderance of functional CL binding to SecYEG, and mediate its roles in ATPase and protein transport activity. In addition, we demonstrate an important role for CL in the conferral of PMF stimulation of protein transport. The apparent transient nature of the CL interaction might facilitate proton exchange with the Sec machinery, and thereby stimulate protein transport, by a hitherto unexplored mechanism. This study demonstrates the power of coupling the high predictive ability of coarse-grained simulation with experimental analyses, toward investigation of both the nature and functional implications of protein–lipid interactions.

SecYEG | protein translocation | molecular dynamics | cardiolipin | native mass spectrometry

The translocation of proteins across and into membranes is an essential process for cell biogenesis and maintenance. Most of this traffic is handled by the conserved Sec translocon. The SecYEG complex conducts proteins through the bacterial plasma membrane either during their synthesis (cotranslationally) or afterward (posttranslationally). The latter pathway is primarily involved in protein secretion, driven by the associated SecA motor protein (Fig. 1*A*). Preproteins engage the complex, involving the insertion of a cleavable N-terminal signal sequence into the SecY lateral gate (LG). Following this, they are passed through a pore in the center of SecY (1, 2) in a process powered by both ATP and the transmembrane proton-motive force (PMF) (3). How ATP binding and hydrolysis drive translocation is currently under debate (4–6), whereas the mechanism of PMF-powered transport is completely unknown.

Like many integral membrane proteins (7, 8), SecYEG is functionally modulated by interactions with specific lipids. Our understanding of these interactions is limited due to the requirement of extracting proteins from their native membrane for purification and characterization, which removes some or all of the natively bound lipids. Various functional studies have addressed this point and show that certain anionic phospholipids, cardiolipin (CL) and phosphatidylglycerol (PG), can stimulate the ATPase activity of SecA, both alone and in complex with SecYEG (9, 10), and, moreover, are important for normal levels of translocation (11, 12). In addition, CL binding has been demonstrated to promote SecYEG dimer formation between adjacent SecE transmembrane helices (TMHs) (10).

SecYEG is not alone in this respect; CL is known to associate with a considerable number of prokaryotic and mitochondrial energy-transducing membrane protein complexes (13). CL has a distinctive structure, comprising two PG molecules joined by a glycerol, resulting in two phosphate head groups with four acyl chains (Fig. 1*B*). It is thought that each phosphate has distinct pK_as (14), resulting in a bicyclic resonance structure at pH 7. This could allow CL to form a proton reservoir, buffering against localized shifts in pH (15), which is potentially important for biological systems involving proton transfer. However, more recent analyses suggest the pK_a values are similar for both phosphates (16, 17), meaning CL would carry a −2 charge at pH 7. How this would affect its ability to shuttle protons is uncertain.

Significance

Many proteins are located in lipid membranes surrounding cells and subcellular organelles. The membrane can impart important structural and functional effects on the protein, making understanding of this interaction critical. Here, we apply computational simulation to the identification of conserved lipid binding sites on an important highly conserved bacterial membrane protein, the Sec translocase (SecA-SecYEG), which uses ATP and the proton-motive force (PMF) to secrete proteins across the bacterial plasma membrane. We experimentally validate these binding sites and use functional analyses to investigate the biological significance of the interactions. We demonstrate that these interactions are specific, transient, and critical for both ATP- and PMF-driven protein secretion.

Author contributions: R.A.C., W.J.A., and I.C. designed research; R.A.C., E.P., W.J.A., D.W.W., and M.C. performed research; R.A.C., E.P., W.J.A., M.C., B.M., I.A., and A.P. analyzed data; and R.A.C., W.J.A., and I.C. wrote the paper.

The authors declare no conflict of interest.

This article is a PNAS Direct Submission.

[1]Present address: Department of Biochemistry, University of Oxford, Oxford OX1 3QU, United Kingdom.

[2]E.P. and W.J.A. contributed equally to this work.

[3]To whom correspondence should be addressed. Email: ian.collinson@bristol.ac.uk.

This article contains supporting information online at www.pnas.org/lookup/suppl/doi:10.1073/pnas.1721536115/-/DCSupplemental.

Published online July 16, 2018.

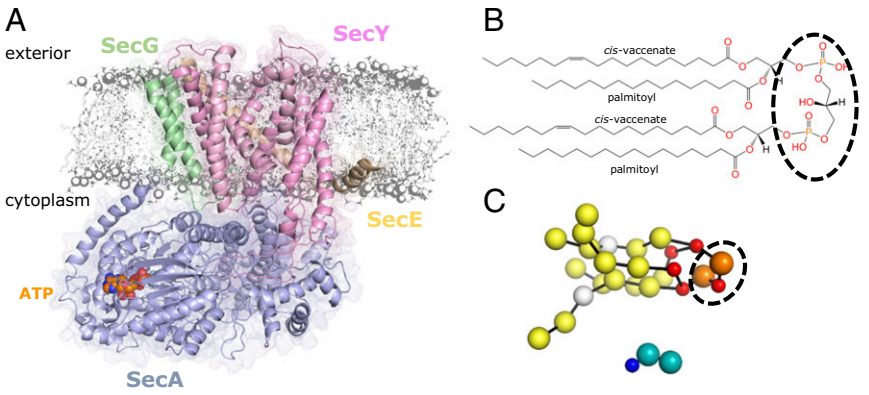

Fig. 1. SecA-SecYEG structure and the MARTINI force field. (*A*) Cartoon of SecYEG bound to SecA, from Protein Data Bank ID code 3DIN (25). The Sec subunits are shown as a cartoon with a mesh overlay, with SecY in light pink, SecE in orange, SecG in green, and SecA in light blue. The ATP analog (ADP-BeFx) is colored as orange, blue, and red spheres. A small region of lipid bilayer is represented in gray. (*B*) Chemical structure of a common CL molecule, in this case, di-1-palmitoyl-2-*cis*-vaccenate-PG. The head group is marked with a black dashed circle. The structure was made using the LIPID MAPS online structure drawing tool (54). (*C*) MARTINI representation of the CL molecule in *B*, with phosphate beads in orange, glycerol beads in red, and acyl tail beads in yellow and white (for beads containing a double bond). The CL head group is marked with a dashed circle as per *B*. Below, a lysine molecule with side-chain beads in light blue and the backbone bead in dark blue is shown. Bonds connecting the beads are shown as black lines.

CL binding sites on proteins are often typified by one or more basic residues that form pockets of positive charge on the surface of the protein (8, 13). This has been observed in structural (18, 19) and simulation data gathered using the MARTINI coarse-grained molecular dynamics (CGMD) force field (20–23). Although of limited atomistic resolution, CGMD is particularly well suited to the identification of protein–lipid interactions (24).

Here, we adapt these analyses toward the identification of CL binding sites in *Thermotoga maritima* SecA-SecYEG (25). The data reveal the presence of two distinct CL binding sites in SecY, as well as supporting a previously reported (5, 26) lipid binding site on the N terminus of SecA. We validate the putative SecY CL binding sites and demonstrate the conserved nature of the SecY–CL interaction using biochemical, native mass spectrometry (nMS), and fluorescence spectroscopy analyses of *Escherichia coli* SecYEG variants.

The precise identification and structural characterization of distinct CL binding sites supersede our previous study (10) and enable interrogation of the functional importance of the SecY–CL interaction. We establish the importance of specific CL binding to the two sites for heightened SecA-SecYEG ATPase and translocation activity, as well as for the stimulation of translocation by the PMF. The results suggest a direct role for CL in the energy-transducing process: an important finding for protein translocation as well as for our general understanding of bioenergetics and membrane transport.

Results

CGMD Simulation Reveals Specific Sec–CL Interactions. We applied the MARTINI coarse-grained force field (22, 23) to predict Sec–CL interactions, using the crystal structure of SecA-SecYEG in a nucleotide-free state as an input model (25) (Fig. 1*A*). In MARTINI, approximately four heavy atoms (i.e., C, P, O, N, etc.) and associated hydrogens are modeled by a single bead, such that CL has 25 beads (Fig. 1*C*) and amino acids have a single backbone bead and up to four beads for the side chain (Fig. 1*C*, blue beads represent a lysine molecule).

The initial analyses followed a "self-assembly" approach, whereby free lipids [with CL at the native level of ∼10% (28, 29)] were allowed to form membranes around the protein over 1-μs simulations. Occupancy analyses over 10 independent simulations reveal key regions of increased CL density around Sec (Fig. 2*A*). To probe these interactions in more detail, the distance between basic residues in SecA-SecYEG and nearby CL head groups was calculated, revealing multiple residues implicated in CL binding, including several with >90% binding occupancy (*SI Appendix*, Fig. S1*A*, red data).

Next, we ran five simulations of SecA-SecYEG in bilayers containing ∼1% CL, chosen to reduce the high occupancy in the self-assembly dataset, thus showing only specific Sec–CL interactions. Each bilayer was simulated for an extended period of up to 55 μs (over 100 μs in total), with rmsd analyses confirming the stability of the simulations (*SI Appendix*, Fig. S1*B*). As above, we determined the CL occupancy for each basic residue in the system, finding a range of 0–11% over the course of the simulation (*SI Appendix*, Fig. S1*A*, blue data).

The combined data highlight several residues at which CL binding occurs (Fig. 2*B*). Of these, the SecY residues K115 and K181 stand out as being highly conserved across different bacterial species (*SI Appendix*, Fig. S2 and Table S1). In addition to these positions, we observe considerable CL binding to the 25 N-terminal residues of SecA ($SecA_N$; *SI Appendix*, Fig. S1*A*), which has previously been shown to be important for lipid binding (5, 26).

Kinetics of CL Binding. Our longer (5–55 μs) simulations permit insight into CL binding kinetics. Distance analyses between K115/K181 and CL head groups reveal several clear binding events (*SI Appendix*, Fig. S3). A detailed analysis of the 55-μs simulation demonstrates that hundreds of binding events occur at both K115 and K181, lasting from ∼100 ns to 2 μs, with a very broad sampling of binding times (*SI Appendix*, Fig. S3). Fitting the data to single exponentials reveals dissociation constants values of ∼4–5 μs^{-1} (*SI Appendix*, Fig. S3, red lines). Kinetics are not always modeled accurately by the MARTINI force field (30); nevertheless, these data clearly indicate that, at native concentrations of CL (∼10% = 70 mM), the on-rate would be very high indeed. Very fast binding and release of CL at the translocon, on the nanosecond to millisecond time scale, is comparable to CL binding to other proteins, including the ATP synthase (20, 21).

Validation of CL Binding Sites by nMS. Plotting a heat map of binding onto basic residues in *T. maritima* SecA-SecYEG reveals that the residues identified above form two distinct sites, termed "site 1" and "site 2" here (Fig. 2*C*). Both sites are typified by the presence of multiple basic residues (*SI Appendix*, Fig. S4*A*). Site 1 comprises the higher CL occupancy residues K103, K115, K118, and R122, all located on TMHs 2–3 of SecY, adjacent to the functionally important SecY LG, the SecA helical scaffold

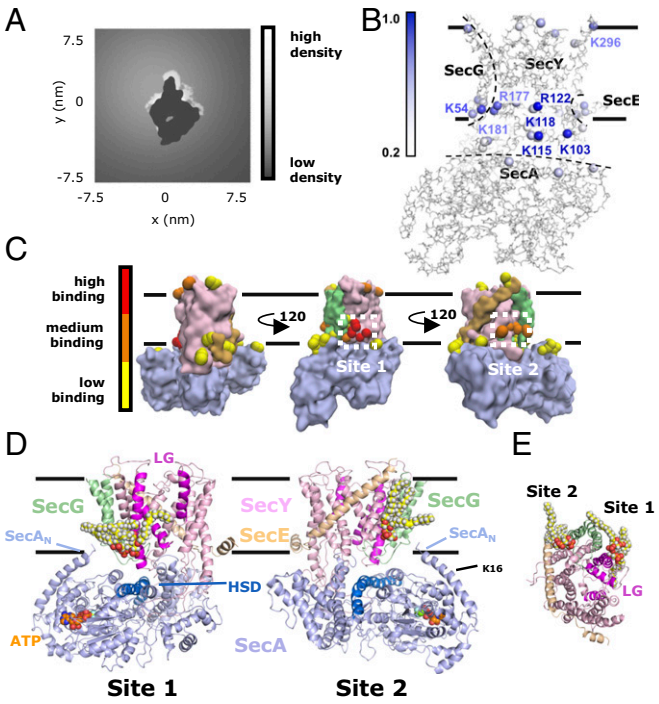

Fig. 2. Identification of SecYEG–CL interactions. (*A*) Density plot of CL head group beads (Fig. 1*C*) in the cytoplasmic leaflet of the membrane, with SecYEG shown in dark gray at the center (SecA removed for clarity). Data were computed for the 10 simulations using the self-assembly method. Distinct CL hotspots can be observed as regions of white around the protein. (*B*) Highest binding basic Sec residues are shown on SecA-SecYEG [Protein Data Bank ID code 3DIN (25)], with the β-carbon atom of each residue colored according to CL occupancy from the datasets in *SI Appendix*, Fig. S1, excluding $SecA_N$. The Sec subunits are approximately demarcated with black dotted lines. (*C*) Views of SecA-SecYEG in MARTINI representation, shown as surfaces and colored as per Fig. 1*A*. CL binding hotspots are shown as spheres and colored according to CL occupancy. Visual analysis reveals two distinct CL binding sites on the cytoplasmic face of SecY, labeled Site 1 and Site 2. (*D*) Two frames from the coarse-grained simulation data, with the protein and bound CL mapped back to an atomistic description (55). SecA-SecYEG is colored as in *C*, except for the SecY LG, shown in magenta, and the SecA HSD, shown in marine. The bound CL is shown as yellow, white, and red spheres. In SecA, the N terminus is labeled [$SecA_N$; Lys-16 is also labeled (K16)] and the crystal structure nucleotide is shown as spheres. (*E*) Same as *D*, but with SecA removed and viewed from the cytoplasm. Both CL binding sites are shown. The molecule has been orientated as per *A*.

domain (HSD), and SecG (Fig. 2*D*). Site 2 comprises K181 and R177 on SecY TMH 4, along with the mid-CL occupancy R15 and R17 on TMH 1. This site is close to the lipid binding $SecA_N$.

To validate and probe conservation of the two CL binding sites, we designed *E. coli* SecYEG variants that abolish the primary positive charges: $SecY^{R113Q,R114Q,K115E,R121Q}EG$ for site 1 and $SecY^{K20Q,R21Q,R22Q,R181E}EG$ for site 2 (*SI Appendix*, Fig. S4*B*), both of which are stable (*SI Appendix*, Fig. S4*C*). Analysis using nMS (31–33) identified SecE, SecG, SecEG, SecY, SecYG, and SecYE (*SI Appendix*, Fig. S5*A*). The intact SecYEG complex was not detected due to the strong collisional activation energy required for removal of detergent from the protein (34).

We saw no CL binding to SecE, SecG, or SecEG, supporting the notion that CL binding occurs mainly to SecY. When using the site 1 and site 2 variants, there was a significant decrease in CL binding to SecY (Fig. 3*A*), validating the assignment of the two CL binding sites from the CGMD. Note that as these substitutions are likely perturbing CL affinity, rather than totally abolishing binding, and that nonspecific CL interactions may be present, the nMS data cannot be used to quantify absolute CL binding at sites 1 and 2. Nevertheless, a qualitative comparison of the variants with wild-type (WT) SecYEG leaves no doubt of a significantly reduced affinity in both cases.

Additional Validation of CL Binding Sites by FRET. To confirm specific CL binding at these sites, we carried out FRET analyses. SecYEG variants with a single cysteine adjacent to either CL site 1 (A103C) or CL site 2 (E18C) were produced in the context of native, Δsite1, and Δsite2 SecYEG, and labeled with Alexa Fluor 350 (Fig. 3*B* and *SI Appendix*, Fig. S5*D*). When a fluorescently labeled CL (TopFluor CL; Avanti) is titrated in, FRET should be observed from the donor (Alexa Fluor 350) to the acceptor. If the sites are specific, a reduction in FRET should be observed when the CL binding site adjacent to a dye is knocked out (A103C and Δsite1, E18C and Δsite2; Fig. 3*B*).

From the titration curves, it is immediately clear that knocking out either CL site reduces the affinity for CL binding (Fig. 3 *C* and *D*). Furthermore, as predicted, Δsite 1 has a stronger effect on A103C (Fig. 3*C*, red data), while Δsite2 has a stronger effect on E18C (Fig. 3*D*, blue data), although, unsurprisingly, there is substantial cross-talk between the sites. To quantify the affinities more precisely, we carried out a global fit of all six datasets, accounting for both the specific and nonspecific FRET (lines in Fig. 3 *C* and *D*, details are provided in *SI Appendix*, *Supplementary Methods*). This allowed us to extract estimates of the affinities for CL at each site, both natively and when knocked out (Fig. 3*E* and *SI Appendix*, Table S6). Under the specific conditions in this experiment [n-Dodecyl-β-D-Maltoside (DDM) micelles, no SecA], we obtain K_ds of ∼3.5 μM for each site, reduced approximately threefold by knocking out the head group binding site.

These FRET results clearly demonstrate the presence of two bona fide CL binding sites rather than just a generalized lowering of CL affinity. While the reductions in affinity appear modest in detergent solution, it should be noted that much of the binding surface comprises acyl chains: In the context of a native membrane, the acyl chains of bound CL are competing with those of the bilayer phospholipids rather than with the less favorable interactions of monoacyl chains of the detergent micelle. Thus, in the membrane, the effects would most likely be more pronounced.

Effect of CL Binding on SecYEG Dimerization. Additional CGMD experiments were set up to probe the role of CL in stabilization of SecYEG dimers (10). Using 16 copies of the *Thermus thermophilus* SecYEG translocon (35) in a membrane with either 0% or 10% CL, it is clear from both visual analysis (*SI Appendix*, Fig. S6*A*) and quantification of dimer formation over time (*SI Appendix*, Fig. S6*B*) that CL is driving SecYEG dimerization, although the dimeric forms observed are highly heterogeneous (*SI Appendix*, Fig. S6*A*). The results suggest that specific CL binding at sites 1 and 2 is not implicated in dimerization (*SI Appendix*, Fig. S6*D*).

Specific CL Binding Increases SecA-SecYEG ATPase Activity. The production of variants with reduced affinity for CL enables analyses of the physiological consequences of the identified SecY–CL interactions (as discussed in this section and beyond). CL binding to SecYEG is known to stimulate the ATPase activity of associated SecA (10), as reinvestigated here. In these experiments, high concentrations of CL have an inhibitory effect (*SI Appendix*, Fig. S7*A*), possibly due to lipid-induced SecA aggregation (10). Therefore, only subsaturating CL concentrations of 0–40 μM could be used for fitting, precluding the determination of apparent K_ds for each variant. Nevertheless, the data could be compared qualitatively by approximate linear fitting. Evidently, the CL stimulation conferred in the site 1 and site 2 variants is reduced by roughly half that of WT SecYEG (Fig. 4*A* and *SI Appendix*, Fig. S7*A*).

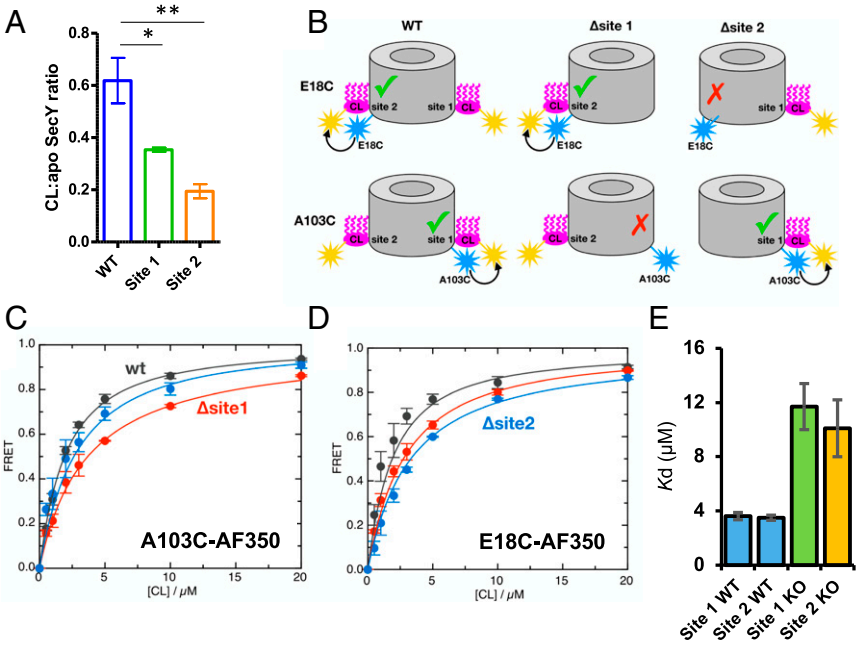

Fig. 3. Experimental validation of CL binding sites. (*A*) Ratios of CL-bound to nonbound (apo) SecY, as measured using nMS, where a value of 1.0 would be equal abundancies of both states. WT SecY has a significantly higher ratio of CL-bound SecY than either the site 1 or site 2 variant (**P* = 0.0194 and ***P* = 0.0048, respectively, using a one-tailed *t* test). Raw data are provided in *SI Appendix*, Fig. S5*A* and Table S3. (*B*) Schematic of the FRET experiment design. SecY (gray) was labeled with Alexa Fluor 350 (blue) adjacent to either site 2 (E18C) or site 1 (A103C). When CL (magenta) labeled with TopFluor (yellow) is able to bind near the label, high FRET occurs (green tick). However, when that specific site is knocked out, the high FRET is abolished (red cross). (*C*) CL titration curves of SecYEG^{A103C}[A350] in native (gray), Δsite1 (red), and Δsite2 (blue) contexts. Error bars represent the SEMs from three independent repeats, and lines show the best global fit (*Materials and Methods*). (*D*) Same as *C*, but for SecYEG^{E18C}[A350]. (*E*) Plots of K_ds from fits in *C* and *D*. Reported are values for each site for both WT systems and the site 1 and 2 knockout variants. Errors are estimated from the fit. Full data are provided in *SI Appendix*, Table S6.

The Role of Specific CL Binding in Protein Transport Through SecYEG. Protein translocation assays, using inverted membrane vesicles (IMVs) made from cells overexpressing SecYEG, show that both variants transport less efficiently, compared with WT (Fig. 4*B* and *SI Appendix*, Fig. S7*B*). Strikingly, while PMF stimulation can be observed in the WT SecYEG IMVs, no PMF stimulation can be observed in either variant. This strongly suggests a role for specific CL binding at sites 1 and 2 in the stimulation of transport by the PMF.

To bolster these data and ensure that the observed lack of PMF stimulation was indeed due to loss of CL binding, we repeated the assay using IMVs from a strain of *E. coli* C43(DE3) devoid of CL (28) (*SI Appendix*, Fig. S7 *C* and *D*). The resultant IMVs retained the ability to harness a PMF via the reverse action of ATP synthase (*SI Appendix*, Fig. S7*E*). Crucially, the translocation data reveal that the IMVs devoid of CL are not stimulated by the PMF (Fig. 4*C* and *SI Appendix*, Fig. S7*F*).

The results signify that specific binding of CL to the sites identified by CGMD analyses is important to both ATP- and PMF-driven transport activity through SecYEG.

Discussion

Integral membrane proteins are strongly affected by the lipid environment in which they reside, through both specific and nonspecific interactions (7, 8). CL is a major component of the energy-conserving membranes of bacteria and mitochondria, intimately associated with resident complexes that couple proton gradients to transport and ATP synthesis/hydrolysis. However, the question remains: By virtue of its special chemistry, does CL act directly in the transmission of protons through energy-transducing membranes?

The bacterial Sec machinery requires CL for efficient translocation (11, 12). Previously, we found two distinct aspects of this dependency: stabilization of the dimeric form of the complex and conferral of high rates of ATP hydrolysis by the associated SecA (10), both of which we have explored further here. Binding of CL to the identified sites 1 and 2 is required for activation of the ATPase activity in SecA, but not for stabilization of SecYEG dimers. The latter is probably brought about by nonspecific interactions and, moreover, is not absolutely essential, as secretion can be driven through one copy of the complex (36). The action of CL at the specific sites is much more interesting.

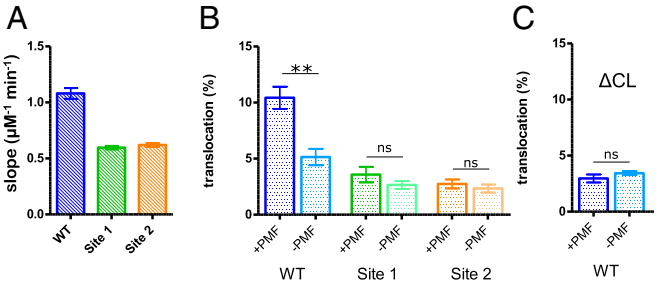

Fig. 4. Physiological implications of SecY–CL interaction. (*A*) ATPase analyses of SecA-SecYEG. Shown are the rates of ATPase increase upon CL addition, as determined from fitting the titration data to linear slopes. Error bars are reported errors for the linear regression. Titration data are provided in *SI Appendix*, Fig. S7*A*. (*B*) In vitro translocation data for IMVs containing overexpressed WT or variant SecYEG. IMVs containing normal levels of CL demonstrate a lower translocation efficiency in the site 1 and site 2 variants, and a total loss of PMF stimulation. PMF knockdown was achieved with a mixture of valinomycin and nigericin. Error bars are SEMs of five repeats, and reported statistical analyses are from one-tailed *t* tests. This analysis clearly shows PMF stimulation in the WT sample (***P* = 0.0024), but not in the variants [*P* = 0.261 and *P* = 0.462 (i.e., not significant [ns])]. (*C*) Same as *B*, but using IMVs with CL biosynthesis knocked out (ΔCL). Here, there is no significant PMF stimulation (*P* = 0.302).

Site 1 is positioned on the edge of the LG, so that the bound CL contacts two of the three LG helices. This suggests possible roles for CL in stabilizing the functionally important open or closed state of the channel (2, 6, 25), or in mediating signal sequence–membrane interactions (37–39). In addition, the proximity of site 1 to residues on the SecA HSD known to be important for lipid binding (40) suggests a role in SecA activation, likely explaining the raised basal ATPase rate of the site 1 variant (*SI Appendix*, Fig. S7*A*). Site 2 is located on the other side of the channel, formed at the SecY-SecG interface. This site is in direct contact with the N terminus of SecA, also previously shown to be important for SecA-membrane binding (5). The CGMD data highlight lysine-16 in this region (Fig. 2*D*, K16), which may well have an important role in SecA activation.

The association of CL at the two sites is also required for PMF stimulation of protein translocation. Thus, membranes lacking CL are incapable of PMF-stimulated translocation. In contrast, the proton transporting ATP synthase retains its activity in these conditions (*SI Appendix*, Fig. S7*E*). Interestingly, secretion clearly occurs in the absence of CL as the triple-CL synthase mutant employed here is nonlethal. Presumably, the cells struggle on with low levels of non–PMF-stimulated secretion activity. The mechanism of this CL-induced activation of SecYEG may be partially structural, bringing negative charges to key sites at the SecYEG-SecA interface, but the effect of CL on PMF stimulation also suggests a more direct role in shuttling protons. Potentially CL molecules could accept protons from a proton wire, such as that observed in SecDF (41); it would then rapidly diffuse them away, facilitated by extremely fast on- and off-rates.

Our results demonstrate the importance of specific protein–lipid interactions to membrane protein structure and function, and the potential of CGMD to identify and probe similar interactions in other energy-transducing, membrane-embedded machines. For the Sec machinery, we find a specific and transient interaction of CL is critical for transport function. Notably, we demonstrate a direct role for CL in the energy-transducing process, rather than simply in protein complex stabilization. This may have implications for the role of CL in other protein complexes.

Materials and Methods

Coarse-Grained Simulations. Simulations of SecA-SecYEG were built using the *T. maritima* crystal structure [Protein Data Bank ID code 3DIN (25)], with the nucleotide removed and missing loops remodeled in Modeler (42). Following this, two distinct setups were used, each described below, with full details of the simulations given in *SI Appendix, Supplementary Methods*.

First, for the self-assembly method, 460 distearoyl phosphoethanolamine and 52 CL molecules [bacterial di-1-palmitoyl-2-*cis*-vaccenate-PG in a −2 charge state (43, 44)] were placed around the protein and allowed to self-assemble into a bilayer. From the following production simulations, frames in which the bilayer had not yet formed, or formed in the *y*–*z* axis in one case, were removed, and the simulations were analyzed for CL density using Visual Molecular Dynamics (VMD) software (Theoretical and Computational Biophysics Group, University of Illinois at Urbana–Champaign).

Second, symmetrical membranes of nine CL and 823 dipalmitoyl phosphatidylcholine molecules were built around the protein beads using insane.py (45), modified here for the inclusion of CL. Rmsd analyses were carried out to ensure the stability of the protein beads (*SI Appendix*, Fig. S1*B*).

In both cases, occupancy analyses were carried through monitoring of CL to residue distances over the time course of the simulation using tools available in the GROMACS package (46).

Protein Expression and Purification. Mutations were introduced using the QuikChange protocol (Stratagene) to *secEYG* in a pBAD expression plasmid. The SecYEG variants were expressed as previously described (47); a full description is provided in *SI Appendix, Supplementary Methods*.

SecA and the model substrate proOmpA were expressed and purified as described previously (48). To facilitate quantification by Western blot analysis, a C-terminal minimal V5 tag (IPNPLLGL) was added to the proOmpA gene by PCR and confirmed by DNA sequencing.

Blue Native PAGE. Blue native PAGE was run using 100 ng of SecYEG in 0.044% DDM in 20 mM Tris (pH 8.0), 130 mM NaCl, and 10% glycerol. CL was added to 30 μM CL, and G250 solution was added to 0.11%. PAGE was run using 3–12% NativePAGE gels (Invitrogen) according to the manufacturer's protocol (i.e., 150 V over 105 min). Gels were then silver-stained using an Invitrogen Silver Quest staining kit, as per the manufacturer's protocol.

Native Mass Spectrometry. Full details of the nMS setup are provided in *SI Appendix, Supplementary Methods*.

The relative abundance of each oligomeric/lipid-bound state of SecYEG was calculated with the Bayesian deconvolution software UniDec (49). Detector efficiency was accounted for before quantification (50). The spectra were analyzed between 3,000 and 8,000 *m/z* to allow quantification of the SecY-based complexes. SecE and SecG monomers were found in the 1,000–3,000-*m/z* range and were discounted from our analysis as they were detected in vast excess to the other oligomeric species. The mass range for peak detection was 45,000–77,000 Da, and species were identified under the following masses: SecY 48,325 ± 50 Da, SecY + CL 49,700 ± 50 Da, SecYG 59,725 ± 50 Da, SecYG + CL 61,125 ± 50 Da, SecYE 63,050 ± 50 Da, SecYE + CL 64,425 ± 50 Da, and SecYEG 74,550 ± 50 Da. The comparison of the apo/CL-bound relative abundances assumes lipid-bound species have similar ionization efficiencies.

For the SecYG and SecYE peaks, no significant difference is seen between the WT and variant SecYEG samples (*SI Appendix*, Fig. S5 *B* and *C*), indicating that the presence of SecE and SecG is able to compensate for the loss of the binding sites on SecY in the site 1 and 2 variants. This is consistent with the observed higher quantities of CL associated with SecYG and SecYE, compared with SecY alone (*SI Appendix*, Tables S3 and S4). Part of this effect is most likely through a contribution of SecE and SecG to the CL binding sites, particularly through provision of hydrophobic subunit interfaces for the acyl tails (e.g., as seen between SecY and SecG in Fig. 2*D*).

FRET Assays. For the FRET experiments, individual cysteines were introduced to otherwise cysteine-free SecYEG by site-directed mutagenesis. Positions were selected to be adjacent to one CL binding site but as far removed as possible from the other: A103C (6) was selected to report on site 1, and E18C was selected to report on site 2 [Fig. 3*B* (schematic) and *SI Appendix*, Fig. S5*D* (structure)]. Each cysteine variant was combined with each CL site mutant, yielding six total combinations: SecYEG^{E18C}, SecYEG$^{E18C}{}_{\Delta site1}$, SecYEG$^{E18C}{}_{\Delta site2}$, SecYEG^{A103C}, SecYEG$^{A103C}{}_{\Delta site1}$, and SecYEG$^{A103C}{}_{\Delta site2}$. These were expressed and purified as described above and then labeled with Alexa Fluor 350 C_5 maleimide (Thermo Fisher Scientific). Labeling efficiencies between 55% and 93% were obtained, assuming molar extinction coefficients of ε_{280} = 70,820 for SecYEG and ε_{346} = 17,000 for Alexa Fluor 350, and a correction factor of 0.19 for dye absorbance at 280 nm.

FRET experiments were performed in a Jobin Yvon FluoroLog spectrofluorometer (Horiba). Emission spectra were measured for 1 μM-labeled SecYEG in standard detergent buffer [20 mM Tris (pH 8.0), 130 mM NaCl, 10% glycerol, 0.02% DDM], with excitation at 350 nm. Next, TopFluor Cardiolipin (1,1′,2,2′-tetraoleoyl CL[4-(dipyrromethene boron difluoride)butanoyl]; Avanti Polar Lipids) solubilized in 0.5% DDM was titrated in.

Full details of the FRET fitting process are provided in *SI Appendix, Supplementary Methods*.

ATPase Assays. In vitro ATPase assays were performed as described previously (48, 51), with full details given in *SI Appendix, Supplementary Methods*.

Preparation of IMVs. IMVs were made from C43(DE3) *E. coli* cells, as well as a C43(DE3) strain in which the three CL synthase genes (*clsA*, *clsB*, and *clsC*) have been knocked out (28). All cells were grown in a modified form of M9 minimal media (12.8 g of Na_2HPO_4, 3 g of KH_2PO_4, 0.5 g of NaCl, 1 g of NH_4Cl, 20 mL of glycerol, 2 mM $MgSO_4$, 100 μM $CaCl_2$, and 10 μM $FeSO_4$). The cells were lysed and centrifuged at 18,000 × *g* for 20 min to clear the lysate, followed by centrifugation on a bed of 20% sucrose at 110,000 × *g* for 2 h. The pellets were resuspended in $TK_{150}M$, homogenized, and run on a stepped sucrose gradient of 0–1.6 M sucrose for ∼16 h at 165,000 × *g*. The IMV band was detected visually, extracted, and diluted in $TK_{150}M$, and it was then centrifuged at 350,000 × *g* for 90 min. The pellets were resuspended in $TK_{150}M$ and aliquoted for storage at −80 °C.

Lipid Quantification Mass Spectrometry. Both sets of cells were grown in M9 minimal medium to OD ∼ 0.8 before induction of WT SecYEG. Five hundred milliliters of cells was harvested at 4,000 × *g*, resuspended in 50 mL of 20 mM Tris (pH 7.5) with 300 mM NaCl, and then centrifuged at 2,500 × *g*. After weight estimation, pellets were resuspended in MilliQ water at a 1:2 mass/volume ratio.

Samples were sonicated for 30 min at 30% power using a 50% pulse. After lipid extraction, as described by Folch et al. (52), phospholipid analysis was performed using liquid chromatography-electrospray ionization-tandem mass spectrometry or HPLC (RSLC Dionex-U3000) equipped with a Corona-CAD Ultra detector coupled to an LTQ-Orbitrap Velos Pro mass spectrometer according to the method of Moulin et al. (53) and supplied by ThermoFisher Scientific.

Note that the C43(DE3) cells were diluted 20-fold for the analysis and that quantification was achieved from the Corona-CAD chromatogram. The ΔCL cells were diluted threefold, and approximate quantification was achieved by extraction of the ionic current in the mass windows corresponding to CL.

Translocation Assays. Transport assays were performed using a modified version of the standard protocol (27), with full details given in *SI Appendix, Supplementary Methods*.

ACKNOWLEDGMENTS. We thank Audrey Solgadi for mass spectrometry analysis at L'Institut Paris Saclay d'Innovation Thérapeutique (IPSIT) and Mikhail Bogdanov for fruitful discussions. This work was funded by the Biotechnology and Biological Sciences Research Council (Grants BB/M003604/1, BB/I008675/1, and BB/N015126/1) and the Wellcome Trust (Grants 104632 and 109854/Z/15/Z). The mass spectrometry work was supported by the Centre National de la Recherche Scientifique, INSERM (Grant "DYNAMO," ANR-11-LABEX-0011-01 to M.C.) and the Région Ile de France for cofunding the Le Service d'Analyse des Médicaments et Métabolites Mass Spectrometry Facility at IPSIT. E.P. is the recipient of an Imperial College London Institute of Chemical Biology Engineering and Physical Sciences Research Council (EPSRC) Centre for Doctoral Training studentship. This work was carried out using the computational facilities of the Advanced Computing Research Centre, University of Bristol. Additional simulations were carried out using Edinburgh Parallel Computing Centre's Cirrus and the ARCHER UK National Supercomputing Service (www.archer.ac.uk), provided by HECBioSim, supported by the EPSRC.

1. Cannon KS, Or E, Clemons WM, Jr, Shibata Y, Rapoport TA (2005) Disulfide bridge formation between SecY and a translocating polypeptide localizes the translocation pore to the center of SecY. *J Cell Biol* 169:219–225.
2. Van den Berg B, et al. (2004) X-ray structure of a protein-conducting channel. *Nature* 427:36–44.
3. Brundage L, Hendrick JP, Schiebel E, Driessen AJM, Wickner W (1990) The purified E. coli integral membrane protein SecY/E is sufficient for reconstitution of SecA-dependent precursor protein translocation. *Cell* 62:649–657.
4. Collinson I, Corey RA, Allen WJ (2015) Channel crossing: How are proteins shipped across the bacterial plasma membrane? *Philos Trans R Soc Lond B Biol Sci* 370: 20150025.
5. Bauer BW, Shemesh T, Chen Y, Rapoport TA (2014) A "push and slide" mechanism allows sequence-insensitive translocation of secretory proteins by the SecA ATPase. *Cell* 157:1416–1429.
6. Allen WJ, et al. (2016) Two-way communication between SecY and SecA suggests a Brownian ratchet mechanism for protein translocation. *eLife* 5:e15598.
7. Lee AG (2003) Lipid-protein interactions in biological membranes: A structural perspective. *Biochim Biophys Acta* 1612:1–40.
8. Palsdottir H, Hunte C (2004) Lipids in membrane protein structures. *Biochim Biophys Acta* 1666:2–18.
9. Lill R, Dowhan W, Wickner W (1990) The ATPase activity of SecA is regulated by acidic phospholipids, SecY, and the leader and mature domains of precursor proteins. *Cell* 60:271–280.
10. Gold VAM, et al. (2010) The action of cardiolipin on the bacterial translocon. *Proc Natl Acad Sci USA* 107:10044–10049.
11. de Vrije T, de Swart RL, Dowhan W, Tommassen J, de Kruijff B (1988) Phosphatidylglycerol is involved in protein translocation across Escherichia coli inner membranes. *Nature* 334:173–175.
12. Kusters R, Dowhan W, de Kruijff B (1991) Negatively charged phospholipids restore prePhoE translocation across phosphatidylglycerol-depleted Escherichia coli inner membranes. *J Biol Chem* 266:8659–8662.
13. Planas-Iglesias J, et al. (2015) Cardiolipin interactions with proteins. *Biophys J* 109: 1282–1294.
14. Kates M, Syz J-Y, Gosser D, Haines TH (1993) pH-dissociation characteristics of cardiolipin and its 2′-deoxy analogue. *Lipids* 28:877–882.
15. Haines TH, Dencher NA (2002) Cardiolipin: A proton trap for oxidative phosphorylation. *FEBS Lett* 528:35–39.
16. Olofsson G, Sparr E (2013) Ionization constants pKa of cardiolipin. *PLoS One* 8:e73040.
17. Sathappa M, Alder NN (2016) The ionization properties of cardiolipin and its variants in model bilayers. *Biochim Biophys Acta* 1858:1362–1372.
18. Ruprecht JJ, et al. (2014) Structures of yeast mitochondrial ADP/ATP carriers support a domain-based alternating-access transport mechanism. *Proc Natl Acad Sci USA* 111: E426–E434.
19. McAuley KE, et al. (1999) Structural details of an interaction between cardiolipin and an integral membrane protein. *Proc Natl Acad Sci USA* 96:14706–14711.
20. Arnarez C, Marrink SJ, Periole X (2013) Identification of cardiolipin binding sites on cytochrome c oxidase at the entrance of proton channels. *Sci Rep* 3:1263.
21. Duncan AL, Robinson AJ, Walker JE (2016) Cardiolipin binds selectively but transiently to conserved lysine residues in the rotor of metazoan ATP synthases. *Proc Natl Acad Sci USA* 113:8687–8692.
22. de Jong DH, et al. (2013) Improved parameters for the Martini coarse-grained protein force field. *J Chem Theory Comput* 9:687–697.
23. Marrink SJ, Risselada HJ, Yefimov S, Tieleman DP, de Vries AH (2007) The MARTINI force field: Coarse grained model for biomolecular simulations. *J Phys Chem B* 111: 7812–7824.
24. Stansfeld PJ, et al. (2015) MemProtMD: Automated insertion of membrane protein structures into explicit lipid membranes. *Structure* 23:1350–1361.
25. Zimmer J, Nam Y, Rapoport TA (2008) Structure of a complex of the ATPase SecA and the protein-translocation channel. *Nature* 455:936–943.
26. Floyd JH, et al. (2014) The dispensability and requirement of SecA N-terminal aminoacyl residues for complementation, membrane binding, lipid-specific domains and channel activities. *Biochem Biophys Res Commun* 453:138–142.
27. Deville K, et al. (2011) The oligomeric state and arrangement of the active bacterial translocon. *J Biol Chem* 286:4659–4669.
28. Carranza G, et al. (2017) Cardiolipin plays an essential role in the formation of intracellular membranes in Escherichia coli. *Biochim Biophys Acta* 1859:1124–1132.
29. Tan BK, et al. (2012) Discovery of a cardiolipin synthase utilizing phosphatidylethanolamine and phosphatidylglycerol as substrates. *Proc Natl Acad Sci USA* 109: 16504–16509.
30. Marrink SJ, Tieleman DP (2013) Perspective on the Martini model. *Chem Soc Rev* 42: 6801–6822.
31. Zhou M, et al. (2011) Mass spectrometry of intact V-type ATPases reveals bound lipids and the effects of nucleotide binding. *Science* 334:380–385.
32. Hernández H, Robinson CV (2007) Determining the stoichiometry and interactions of macromolecular assemblies from mass spectrometry. *Nat Protoc* 2:715–726.
33. Heck AJ (2008) Native mass spectrometry: A bridge between interactomics and structural biology. *Nat Methods* 5:927–933.
34. Laganowsky A, Reading E, Hopper JT, Robinson CV (2013) Mass spectrometry of intact membrane protein complexes. *Nat Protoc* 8:639–651.
35. Tanaka Y, et al. (2015) Crystal structures of SecYEG in lipidic cubic phase elucidate a precise resting and a peptide-bound state. *Cell Reports* 13:1561–1568.
36. Park E, Rapoport TA (2012) Bacterial protein translocation requires only one copy of the SecY complex in vivo. *J Cell Biol* 198:881–893.
37. Hizlan D, et al. (2012) Structure of the SecY complex unlocked by a preprotein mimic. *Cell Rep* 1:21–28.
38. Briggs MS, Cornell DG, Dluhy RA, Gierasch LM (1986) Conformations of signal peptides induced by lipids suggest initial steps in protein export. *Science* 233:206–208.
39. McKnight CJ, Stradley SJ, Jones JD, Gierasch LM (1991) Conformational and membrane-binding properties of a signal sequence are largely unaltered by its adjacent mature region. *Proc Natl Acad Sci USA* 88:5799–5803.
40. Cooper DB, et al. (2008) SecA, the motor of the secretion machine, binds diverse partners on one interactive surface. *J Mol Biol* 382:74–87.
41. Tsukazaki T, et al. (2011) Structure and function of a membrane component SecDF that enhances protein export. *Nature* 474:235–238.
42. Fiser A, Do RK, Sali A (2000) Modeling of loops in protein structures. *Protein Sci* 9: 1753–1773.
43. Dahlberg M, Maliniak A (2010) Mechanical properties of coarse-grained bilayers formed by cardiolipin and zwitterionic lipids. *J Chem Theory Comput* 6:1638–1649.
44. Dahlberg M (2007) Polymorphic phase behavior of cardiolipin derivatives studied by coarse-grained molecular dynamics. *J Phys Chem B* 111:7194–7200.
45. Wassenaar TA, Ingólfsson HI, Böckmann RA, Tieleman DP, Marrink SJ (2015) Computational lipidomics with insane: A versatile tool for generating custom membranes for molecular simulations. *J Chem Theory Comput* 11:2144–2155.
46. Berendsen HJC, van der Spoel D, van Drunen R (1995) GROMACS: A message-passing parallel molecular dynamics implementation. *Comput Phys Commun* 91:43–56.
47. Collinson I, et al. (2001) Projection structure and oligomeric properties of a bacterial core protein translocase. *EMBO J* 20:2462–2471.
48. Gold VAM, Robson A, Clarke AR, Collinson I (2007) Allosteric regulation of SecA: Magnesium-mediated control of conformation and activity. *J Biol Chem* 282: 17424–17432.
49. Marty MT, et al. (2015) Bayesian deconvolution of mass and ion mobility spectra: From binary interactions to polydisperse ensembles. *Anal Chem* 87:4370–4376.
50. Fraser G (2002) The ion detection efficiency of microchannel plates (MCPs). *Int J Mass Spectrom* 215:13–30.
51. Corey RA, et al. (2016) Unlocking the bacterial SecY translocon. *Structure* 24:518–527.
52. Folch J, Lees M, Sloane Stanley GH (1957) A simple method for the isolation and purification of total lipides from animal tissues. *J Biol Chem* 226:497–509.
53. Moulin M, et al. (2015) Sex-specific cardiac cardiolipin remodelling after doxorubicin treatment. *Biol Sex Differ* 6:20.
54. Fahy E, Sud M, Cotter D, Subramaniam S (2007) LIPID MAPS online tools for lipid research. *Nucleic Acids Res* 35(Suppl 2):W606–W612.
55. Wassenaar TA, Pluhackova K, Böckmann RA, Marrink SJ, Tieleman DP (2014) Going backward: A flexible geometric approach to reverse transformation from coarse grained to atomistic models. *J Chem Theory Comput* 10:676–690.